

# Revisiting Hydrometeorology Using Cloud and Climate Observations

ALAN K. BETTS

*Atmospheric Research, Pittsford, Vermont*

AHMED B. TAWFIK

*National Center for Atmospheric Research, Boulder, Colorado*

RAYMOND L. DESJARDINS

*Agriculture and Agri-Food Canada, Ottawa, Ontario, Canada*

(Manuscript received 24 August 2016, in final form 30 December 2016)

## ABSTRACT

This paper uses 620 station years of hourly Canadian Prairie climate data to analyze the coupling of monthly near-surface climate with opaque cloud, a surrogate for radiation, and precipitation anomalies. While the cloud–climate coupling is strong, precipitation anomalies impact monthly climate for as long as 5 months. The April climate has memory of precipitation anomalies back to freeze-up in November, mostly stored in the snowpack. The summer climate has memory of precipitation anomalies back to the beginning of snowmelt in March. In the warm season, mean temperature is strongly correlated to opaque cloud anomalies, but only weakly to precipitation anomalies. Mixing ratio anomalies are correlated to precipitation, but only weakly to cloud. The diurnal cycle of mixing ratio shifts upward with increasing precipitation anomalies. Positive precipitation anomalies are coupled to a lower afternoon lifting condensation level and a higher afternoon equivalent potential temperature; both favor increased convection and precipitation. Regression coefficients on precipitation increase from wet to dry conditions. This is consistent with increased uptake of soil water when monthly precipitation is low, until drought conditions are reached, and also consistent with gravity satellite observations. Regression analysis shows monthly opaque cloud cover is tightly correlated to three climate variables that are routinely observed: diurnal temperature range, mean temperature, and mean relative humidity. The set of correlation coefficients, derived from cloud and climate observations, could be used to evaluate the representation of the land–cloud–atmosphere system in both forecast and climate models.

## 1. Introduction

The coupling between the energy and water cycles at the land surface is central to hydrometeorology and important to weather forecasts on time scales from days to seasons. On daily time scales, the land–atmosphere system is fully coupled, so errors in the model representation of processes in the soil, vegetation, boundary layer, and cloud fields can rapidly bias a model forecast. An earlier review, [Betts \(2004\)](#), looked at hydrometeorology from the global modeling perspective using model reanalysis data. These model data showed how net longwave and shortwave radiation, cloud cover, surface fluxes, diurnal temperature range, soil moisture,

and cloud-base height were coupled on daily time scales over river basins.

Historically, the observed climate variables available to understand land surface–atmosphere coupling were temperature and precipitation, along with pressure, wind, relative humidity, and snow depth. Other key variables such as longwave (LW) and shortwave (SW) radiation, soil moisture, and soil temperature, and the surface sensible and latent heat fluxes are only available at a more limited number of flux sites ([Baldocchi 2003](#); [Xie et al. 2010](#)). Initially, these measurements were available from summer field experiments, but in the last decade or so they have become available on a continuous basis, which makes them increasingly valuable for analyzing cloud–atmosphere–land coupling.

Recent work using the Canadian Prairie data, an hourly dataset going back 60 years with little missing

---

*Corresponding author e-mail:* Alan K. Betts, akbetts@aol.com

data, has given us powerful new observational insights into hydrometeorology on climate time scales (Betts et al. 2013a,b, 2014a,b, 2015, 2016; Betts and Tawfik 2016). The primary reason is that, in addition to the conventional World Meteorological Organization cloud observations, trained observers recorded hourly the fraction of the sky in tenths covered by opaque, reflective clouds that obscured the sun, moon, or stars. As daily and daytime means, these opaque cloud observations can be calibrated to give the  $LW_{net}$  and the SW cloud forcing, using the baseline surface radiation network (BSRN 2016) station on the Prairies, 25 km south of Regina in Saskatchewan (Betts et al. 2015). These opaque cloud observations are thus a surrogate for LW and SW cloud forcing (LWCF and SWCF), which determine much of the variability in the fully coupled land surface–cloud system on daily and longer time scales (Betts et al. 2014a; Betts and Tawfik 2016). It is probably fair to say that without the cloud forcing of the land surface, our long-term climate and hydrological analyses have had critical limitations. Of course, global models have all the radiation terms, but they are subject to the uncertainties in the model clouds and their radiative properties, and this leads to substantial differences between model climate simulations, especially in climate sensitivity estimates (Webb et al. 2006, 2013).

Many modeling studies have shown a link between increased soil moisture anomalies and both cloud and precipitation (e.g., Betts et al. 1996; Fennessy and Shukla 1999; Koster and Suarez 2001; Pal and Eltahir 2001; Betts 2004; Ek and Holtslag 2004; Wu et al. 2007; Kim and Wang 2007; Koster and Manahama 2012; Ferguson et al. 2012). Some of the listed works found that relatively dry spring soil moisture conditions resulted in less summer rainfall and warmer temperatures, while wetter spring soil moisture conditions had either weak or no effects. A multimodel assessment of seasonal and subseasonal predictability was later conducted during phase 2 of the Global Land–Atmosphere Coupling Experiment (GLACE-2; Koster et al. 2010, 2011). GLACE-2 found that subseasonal forecasts of 2-m air temperature could be improved by including more realistic soil moisture initialization. Precipitation forecasts show much weaker benefits over the contiguous United States, however. GLACE-2 also pointed out the asymmetry in dry versus wetter initializations, suggesting that the northern plains showed improved skill under drier conditions, while the southwestern United States showed increased forecast skill when soils were wetter. A recent observational study (Tuttle and Salvucci 2016) suggests that this feedback is complex and may change sign between the western and eastern United States, which they attributed to regional aridity. The GLACE-2

study over Europe (Van den Hurk et al. 2012) showed that realistic soil moisture assimilation improved temperature forecast skill up to 6 weeks, but there was little improvement in precipitation forecast skill.

The Canadian Prairie data show an increase of station precipitation with the intensification of land use that resulted from a 20% reduction of the land area that was left fallow in the growing season (Betts et al. 2013b, 2016), and some increase with decreasing wind speed and increased equivalent potential temperature in summer (Betts and Tawfik 2016). However, the regression of monthly precipitation anomalies on precipitation anomalies for preceding months in summer shows no correlation (Betts et al. 2014a). This suggests that the link between current and lagged monthly precipitation anomalies, soil moisture anomalies, and evaporation on monthly time scales may not be simple. One confounding factor is that the extraction of soil water over the growing season from May to August (MJJ), estimated from the reduction in total water storage, is a large damping factor on wet or dry precipitation anomalies (Betts et al. 2014a). Section 4e of this analysis will show a similar damping in the correlation coefficients with increasing precipitation anomalies.

The Prairie dataset is sufficiently large (more than 600 station years) and of sufficient quality that we can describe the land surface coupling both on the diurnal time scale (Betts and Tawfik 2016) and on the monthly time scale (Betts et al. 2014a). This paper is an extension of Betts et al. (2014a), in which we extract the monthly mean diurnal cycles following Betts and Tawfik (2016) rather than approximate them, and then look more deeply at the coupling between the near-surface thermodynamic variables and anomalies of opaque cloud and precipitation. On monthly time scales, we can use multiple linear regressions to extract the correlation coefficients between anomalies of temperature and humidity (and derived variables) and anomalies of cloud and precipitation for the current and previous months (see section 2).

In this northern latitude Prairie climate, during the warm season from May to October snow is rare, and during the cold season from November to March/April snow cover is common. The climate transitions with snow cover are fast and dramatic: temperature drops 10 K as a result of the high albedo of surface snow, a fall in the downward LW radiation, and a shift to a stable boundary layer (Betts et al. 2014b; Betts and Tawfik 2016). In section 3, we will show how the mean thermodynamic fields in April have memory of precipitation back through the entire cold season to November. In section 4, we will explore many aspects of the coupling in the warm season. First, we show that during July and August, some humidity variables and the afternoon height of the lifting

condensation level (LCL) show memory of precipitation anomalies back to March. This extended memory suggests that improvements in seasonal forecasting may be possible. Then, we merge the months May–August to develop a set of correlation coefficients broadly representative of the growing season and show the warm season climate dependence on opaque cloud and precipitation. We show how the diurnal cycle of mixing ratio, with two maxima and minima, depends on cloud and precipitation anomalies. Finally, we show how the correlation coefficients themselves change with precipitation anomalies from dry to wet conditions. In section 5, we look briefly at the inverse problem: how well opaque cloud cover can be determined from climate variables. Section 6 presents our conclusions.

## 2. Data processing and methodology

### a. Canadian Prairie dataset

For this paper we analyze six Canadian Prairie stations in Alberta (Calgary, Lethbridge, Medicine Hat, Edmonton, Red Deer, and Grande Prairie) and six stations in Saskatchewan (Estevan, Regina, Moose Jaw, Swift Current, Saskatoon, and Prince Albert). The period of record is 1953–2010; however, some stations had no precipitation records from 2005 to 2010 (see Betts et al. 2014a), and most snow-depth data were only available from 1955 to 2006 (Betts et al. 2014b). Approximately 620 station years of data were available. Station identifiers, location, and elevation are given in Table 1 in Betts and Tawfik (2016), together with a map showing their location and the land cover. Eleven stations, with typical station spacing on the order of 150 km, are in an agricultural region with an east–west domain of 720 km and north–south domain of 480 km. The twelfth station, Grande Prairie, is about 350 km to the west-northwest of Edmonton. There has been some land-use change over the 58-yr period, as the practice of summer fallowing has been replaced with continuous cropping in many regions (Betts et al. 2013b); however, for this study, we will merge all years. The main annual crops are canola and cereal crops such as wheat and barley, and some pulse crops such as peas and lentils.

The hourly data were processed as intact monthly mean diurnal cycles for each station for each year. The time base is local standard time. The hourly dataset is remarkably complete. Days were only omitted if <20 h of data were available. Months were omitted if they had fewer than 28 days remaining, except for February, where this threshold was reduced to 25 days.

From the monthly diurnal cycles of temperature  $T$  and relative humidity (RH) and station pressure  $P_S$  data, we

computed a set of derived thermodynamic variables, mixing ratio  $Q$ , equivalent potential temperature  $\theta_E$ , and pressure height to the lifting condensation level  $P_{LCL}$ .

For each variable  $Y$ , we extracted from the monthly mean diurnal cycles (Betts and Tawfik 2016) the daily mean  $Y_m$ , the maximum and minimum ( $Y_x$  and  $Y_n$ , respectively), and the times of the maximum and minimum. We then computed the long-term station monthly mean and used these to compute monthly anomalies  $\delta Y$ . For the daily precipitation and snow depth, we also computed monthly means, the long-term station monthly means, and used these to compute monthly anomalies for each station. We computed a monthly snow cover frequency as the fraction of days in a month with snow depth  $>0$ , and again calculated anomalies from the long-term station means.

The monthly anomalies of opaque cloud, precipitation, snow depth, and snow cover frequency were then standardized by their monthly standard deviation (SD). For the temperature anomalies  $\delta T_m$ ,  $\delta T_x$ , and  $\delta T_n$  and the diurnal temperature range  $\delta DTR$ , we standardized by the monthly SD of  $\delta T_m$ . Similarly for the variables  $\delta RH_m$ ,  $\delta RH_x$ , and  $\delta RH_n$  and the diurnal RH range  $\delta DRHR$ , we standardized by the monthly SD of  $\delta RH_m$ . The corresponding set of anomalies for equivalent potential temperature  $\delta\theta_E$  and pressure height to the lifting condensation level  $\delta P_{LCL}$  were standardized by the monthly SD of  $\delta\theta_{Em}$  and  $\delta P_{LCLm}$ , respectively.

We first analyzed individual stations, then merged the Alberta and Saskatchewan station groups and found similar results. Consequently, we merged all 12 stations to present the results in this paper. These data are available from Environment and Climate Change Canada (<http://climate.weather.gc.ca/>) or from the corresponding author.

### b. Standardized multiple regression

We used multiple linear regression to explore the correlation between variables. Following Betts et al. (2014a), our starting format was to regress a standardized (denoted  $\sigma$ ) thermodynamic anomaly  $\delta Y_\sigma$  on mean opaque cloud anomalies  $\delta OPAQ_{m\sigma}$  for the current month and lagged precipitation anomalies for the current month  $\delta PR_{0\sigma}$  and preceding months ( $\delta PR_{1\sigma}$ ,  $\delta PR_{2\sigma}$ ,  $\delta PR_{3\sigma}$ ,  $\dots$ ,  $\delta PR_{5\sigma}$ ) in the form

$$\delta Y_\sigma = K + A(\delta OPAQ_{m\sigma}) + B(\delta PR_{0\sigma}) + C(\delta PR_{1\sigma}) + D(\delta PR_{2\sigma}) + E(\delta PR_{3\sigma}) + \dots + G(\delta PR_{5\sigma}). \quad (1)$$

Multiple regression shows no memory of cloud for previous months. Since we are using anomalies, the leading coefficient  $K$  is of order zero and will not be shown.

TABLE 1. Mean local times (LST) for diurnal cycle maxima and minima for six stations in Saskatchewan.

Month (count)	$T_n$	$T_x$	$RH_x$	$RH_n$	$\theta_{Ex}$
April (300)	5.69 ± 0.53	15.77 ± 0.73	5.59 ± 1.08	15.79 ± 1.15	15.76 ± 0.78
May (301)	5.07 ± 0.60	15.82 ± 0.85	5.39 ± 0.71	15.98 ± 1.20	15.67 ± 0.97
June (298)	4.71 ± 0.55	15.78 ± 0.96	4.98 ± 0.65	15.90 ± 1.21	15.52 ± 1.32
July (297)	4.96 ± 0.59	15.82 ± 0.87	5.10 ± 0.69	15.94 ± 1.13	15.69 ± 1.43
August (299)	5.67 ± 0.54	15.78 ± 0.73	5.67 ± 0.60	16.03 ± 0.92	15.22 ± 1.23
September (298)	6.40 ± 0.68	15.54 ± 0.68	6.41 ± 0.82	15.72 ± 0.96	15.19 ± 0.88
October (297)	6.71 ± 0.66	15.15 ± 0.66	6.78 ± 0.94	15.31 ± 0.73	14.93 ± 0.69
MJJA mean	5.10 ± 0.67	15.80 ± 0.85	5.28 ± 0.71	15.96 ± 1.12	15.52 ± 1.26

Total opaque cloud was observed and recorded in units of tenths of the sky, which we converted to a fraction (0–1) of sky cover. Precipitation was recorded in millimeters per day, and snow depth in centimeters. After standardization, all variables are dimensionless, but for graphs, we will often multiply by the SD used for standardization to recover the dimensional units.

### c. Significance of multiple regression coefficients

In the tables reporting the  $A$ – $G$  coefficients corresponding to Eq. (1), coefficients with >99% confidence ( $p < 0.01$  based on a Student's  $t$  test for significance) are boldface, coefficients with 95%–99% confidence ( $0.01 \leq p < 0.05$ ) are roman, coefficients with 90%–95% confidence ( $0.05 \leq p < 0.1$ ) are italicized, and coefficients with <90% confidence are listed in parentheses. Tables also show the adjusted coefficient of determination  $R^2$  values and the number of months in each analysis. As the correlation coefficients with lagged precipitation anomalies decrease going back to earlier months, their contribution to increasing  $R^2$  values become small, even though the regression coefficients remain significant because of our large sample size. For the warm season months MJJA, some humidity variables show memory of precipitation anomalies back to March (see section 4). For April, the time of snowmelt and ground ice melt, there is memory of precipitation anomalies going back for the entire cold season to November (see section 3).

### d. Conceptual issues

Multiple regression gives us correlation coefficients between sets of variables [and an estimate of their root-mean-square (RMS) uncertainty and a confidence estimate], but since this is a fully coupled system, we cannot address questions of cause and effect. Our choice of predicted and predictor variables is based on a conceptual model. For example, we shall start with regressing all the 2-m thermodynamic variables on opaque cloud and lagged precipitation, looking at the patterns, and especially for the variables like DTR and  $RH_n$  that have tight relationships (large regression  $R^2$ ). Precipitation comes from clouds, but it is intermittent, as many days

have no precipitation. Our monthly warm season analysis uses current monthly precipitation and precipitation for the preceding months, going back until the coefficients in Eq. (1) become as small as the estimate of their RMS, when  $R^2$  values no longer increase. But given the key role of cloud forcing and the uncertainty in cloud properties in models, we will ask the inverse question in section 5: how well are cloud anomalies known, given climate variable anomalies.

There are known physical constraints on the coupling of parameters. The radiative forcing by opaque clouds is a strong driver of the diurnal cycle of  $T$  and RH (Betts et al. 2013a). Relative humidity is a key variable in the coupled land–atmosphere system. The fall of  $T_n$  is limited if saturation is reached at night. The daily mean  $RH_m$  is linked to vegetative resistance to transpiration, which drops RH from saturation inside the leaf to its value in the near-surface layer (Betts et al. 2004). Once the boundary layer (BL) grows through the nighttime stable inversion a few hours after sunrise, the LCL is typically tied to cloud-base pressure and to the depth of the mixed layer (ML). Cloud-base temperature determines the downward longwave radiation from the BL cloud field, which is a tightly coupled component of the LWCF. Cloud-base pressure, temperature, and mixing ratio determine the moist adiabat (i.e.,  $\theta_E$ ) for ascending parcels, as well as cloud liquid water that feeds the development of precipitation. Mixing ratio (i.e.,  $Q$ ) can be calculated from  $T$  and RH, so when the regression shows (see section 4a) that afternoon  $Q$  is correlated to precipitation, rather than to cloud forcing, this imposes a constraint on  $T$  and RH at the afternoon temperature maximum.

### e. Timing of diurnal cycle

Our methodology is based on the climatology of the monthly mean diurnal cycle from which we extract the mean, maxima, and minima. This works well for  $T$ , RH,  $P_{LCL}$ , and  $\theta_E$ , which have a single maxima and minima, but not for  $Q$ , which has two maxima and minima in the warm season, unless it is very cloudy (Betts et al. 2013a; Betts and Tawfik 2016). Table 1 shows the mean and

TABLE 2. Standardized regression coefficients for April anomalies  $\delta\text{DTR}_{\sigma}$ ,  $\delta T_{x\sigma}$ ,  $\delta\text{RH}_{n\sigma}$ ,  $\delta\text{RH}_{m\sigma}$ , and  $\delta\text{P}_{\text{LCLX}\sigma}$  on standardized anomalies of opaque cloud and precipitation, adding March snow-depth anomalies, and adding fraction of April days with snow cover. For coefficients, boldface represents  $p < 0.01$  ( $>99\%$ ), roman represents  $0.01 \leq p < 0.05$ , italic represents  $0.05 \leq p < 0.1$ , and parentheses represent  $p > 0.1$ .

Variable	$\delta\text{DTR}_{\sigma}$	$\delta T_{x\sigma}$	$\delta\text{RH}_{n\sigma}$	$\delta\text{RH}_{m\sigma}$	$\delta\text{P}_{\text{LCLX}\sigma}$
Opaque cloud and precipitation					
620 months $R^2$	0.67	0.47	0.65	0.63	0.66
$\delta\text{OPAQ}_m\text{-Apr}_{\sigma}$ (A)	<b><math>-0.52 \pm 0.02</math></b>	<b><math>-0.78 \pm 0.04</math></b>	<b><math>0.76 \pm 0.03</math></b>	<b><math>0.60 \pm 0.03</math></b>	<b><math>-0.93 \pm 0.04</math></b>
$\delta\text{PR- Apr}_{\sigma}$ (B)	<b><math>-0.06 \pm 0.02</math></b>	( $0.01 \pm 0.04$ )	<b><math>0.20 \pm 0.03</math></b>	<b><math>0.17 \pm 0.03</math></b>	<b><math>-0.19 \pm 0.04</math></b>
$\delta\text{PR- Mar}_{\sigma}$ (C)	<b><math>-0.12 \pm 0.02</math></b>	<b><math>-0.22 \pm 0.04</math></b>	<b><math>0.23 \pm 0.03</math></b>	<b><math>0.19 \pm 0.02</math></b>	<b><math>-0.27 \pm 0.03</math></b>
$\delta\text{PR- Feb}_{\sigma}$ (D)	<b><math>-0.07 \pm 0.02</math></b>	<b><math>-0.12 \pm 0.04</math></b>	<b><math>0.16 \pm 0.03</math></b>	<b><math>0.13 \pm 0.02</math></b>	<b><math>-0.19 \pm 0.03</math></b>
$\delta\text{PR- Jan}_{\sigma}$ (E)	<b><math>-0.09 \pm 0.02</math></b>	<b><math>-0.19 \pm 0.04</math></b>	<b><math>0.17 \pm 0.03</math></b>	<b><math>0.13 \pm 0.02</math></b>	<b><math>-0.21 \pm 0.03</math></b>
$\delta\text{PR- Dec}_{\sigma}$ (F)	<b><math>-0.06 \pm 0.02</math></b>	( $-0.06 \pm 0.04$ )	<b><math>0.16 \pm 0.03</math></b>	<b><math>0.14 \pm 0.02</math></b>	<b><math>-0.19 \pm 0.03</math></b>
$\delta\text{PR- Nov}_{\sigma}$ (G)	<b><math>-0.08 \pm 0.02</math></b>	<b><math>-0.13 \pm 0.04</math></b>	$0.07 \pm 0.03$	<b><math>0.08 \pm 0.02</math></b>	<b><math>-0.11 \pm 0.03</math></b>
Adding March snow-depth anomalies					
552 months $R^2$	0.70	0.46	0.71	0.67	0.71
$\delta\text{OPAQ}_m\text{-Apr}_{\sigma}$ (A)	<b><math>-0.53 \pm 0.02</math></b>	<b><math>-0.74 \pm 0.05</math></b>	<b><math>0.77 \pm 0.03</math></b>	<b><math>0.61 \pm 0.03</math></b>	<b><math>-0.95 \pm 0.04</math></b>
$\delta\text{PR- Apr}_{\sigma}$ (B)	<b><math>-0.06 \pm 0.02</math></b>	( $-0.02 \pm 0.05$ )	<b><math>0.21 \pm 0.03</math></b>	<b><math>0.18 \pm 0.03</math></b>	<b><math>-0.21 \pm 0.04</math></b>
$\delta\text{PR- Mar}_{\sigma}$ (C)	<b><math>-0.09 \pm 0.02</math></b>	<b><math>-0.17 \pm 0.04</math></b>	<b><math>0.17 \pm 0.03</math></b>	<b><math>0.14 \pm 0.03</math></b>	<b><math>-0.20 \pm 0.04</math></b>
$\delta\text{PR- Feb}_{\sigma}$ (D)	<i><math>-0.03 \pm 0.02</math></i>	( $-0.04 \pm 0.04$ )	( $0.04 \pm 0.03$ )	$0.06 \pm 0.03$	<i><math>-0.06 \pm 0.04</math></i>
$\delta\text{PR- Jan}_{\sigma}$ (E)	<b><math>-0.05 \pm 0.02</math></b>	$-0.09 \pm 0.04$	$0.07 \pm 0.03$	$0.06 \pm 0.03$	$-0.09 \pm 0.04$
$\delta\text{PR- Dec}_{\sigma}$ (F)	$-0.04 \pm 0.02$	( $-0.02 \pm 0.04$ )	<b><math>0.12 \pm 0.03</math></b>	<b><math>0.12 \pm 0.02</math></b>	<b><math>-0.15 \pm 0.03</math></b>
$\delta\text{PR- Nov}_{\sigma}$ (G)	<b><math>-0.05 \pm 0.02</math></b>	<b><math>-0.12 \pm 0.04</math></b>	( $0.01 \pm 0.03$ )	( $0.03 \pm 0.03$ )	( $-0.03 \pm 0.03$ )
$\delta\text{Snowdepth- Mar}_{\sigma}$ (S)	<b><math>-0.13 \pm 0.02</math></b>	<b><math>-0.19 \pm 0.05</math></b>	<b><math>0.34 \pm 0.04</math></b>	<b><math>0.24 \pm 0.03</math></b>	<b><math>-0.39 \pm 0.04</math></b>
Adding fraction of April days with snow cover					
550 months $R^2$	0.73	0.65	0.80	0.70	0.78
$\delta\text{OPAQ}_m\text{-Apr}_{\sigma}$ (A)	<b><math>-0.49 \pm 0.02</math></b>	<b><math>-0.57 \pm 0.04</math></b>	<b><math>0.65 \pm 0.03</math></b>	<b><math>0.54 \pm 0.03</math></b>	<b><math>-0.82 \pm 0.04</math></b>
$\delta\text{PR- Apr}_{\sigma}$ (B)	$-0.04 \pm 0.02$	( $0.03 \pm 0.04$ )	<b><math>0.16 \pm 0.03</math></b>	<b><math>0.15 \pm 0.03</math></b>	<b><math>-0.15 \pm 0.04</math></b>
$\delta\text{PR- Mar}_{\sigma}$ (C)	<b><math>-0.08 \pm 0.02</math></b>	$-0.07 \pm 0.03$	<b><math>0.14 \pm 0.03</math></b>	<b><math>0.14 \pm 0.03</math></b>	<b><math>-0.18 \pm 0.03</math></b>
$\delta\text{PR- Feb}_{\sigma}$ (D)	<b><math>-0.05 \pm 0.02</math></b>	( $-0.02 \pm 0.03$ )	<b><math>0.09 \pm 0.03</math></b>	<b><math>0.10 \pm 0.03</math></b>	<b><math>-0.11 \pm 0.03</math></b>
$\delta\text{PR- Jan}_{\sigma}$ (E)	<b><math>-0.05 \pm 0.02</math></b>	( $0.01 \pm 0.03$ )	$0.06 \pm 0.03$	<b><math>0.07 \pm 0.03</math></b>	<b><math>-0.08 \pm 0.03</math></b>
$\delta\text{PR- Dec}_{\sigma}$ (F)	<b><math>-0.04 \pm 0.02</math></b>	( $0.00 \pm 0.03$ )	<b><math>0.12 \pm 0.02</math></b>	<b><math>0.13 \pm 0.02</math></b>	<b><math>-0.16 \pm 0.03</math></b>
$\delta\text{PR- Nov}_{\sigma}$ (G)	<b><math>-0.06 \pm 0.02</math></b>	<b><math>-0.10 \pm 0.03</math></b>	( $0.01 \pm 0.02$ )	( $0.04 \pm 0.02$ )	( $-0.04 \pm 0.03$ )
$\delta\text{Snowcover- Apr}_{\sigma}$ (T)	<b><math>-0.19 \pm 0.02</math></b>	<b><math>-0.63 \pm 0.04</math></b>	<b><math>0.52 \pm 0.03</math></b>	<b><math>0.31 \pm 0.03</math></b>	<b><math>-0.57 \pm 0.03</math></b>

standard deviation by month for the local times of  $T_n$ ,  $T_x$ ,  $\text{RH}_x$ ,  $\text{RH}_n$ , and  $\theta_{\text{Ex}}$  for a merge of the six stations in Saskatchewan. The times for  $T_n$  and  $\text{RH}_x$  occur near sunrise, which varies by month, but the times of afternoon  $T_x$ ,  $\text{RH}_n$ , and  $\theta_{\text{Ex}}$  vary little from April to September. The times of afternoon maximum and minimum across these variables coincide within the hourly resolution of the raw data and the monthly standard deviations shown.

For mixing ratio  $Q$ , we can easily compute the daily mean, but given the more complex double mode diurnal structure, we recomputed values  $Q_{\text{Tn}}$  and  $Q_{\text{Tx}}$  from the morning pairs near sunrise  $T_n$ ,  $\text{RH}_x$  and afternoon pairs near the maximum temperature  $T_x$ ,  $\text{RH}_n$ . The full diurnal cycle of  $Q$  will be shown in section 4d.

### 3. Memory in April climatology of cold season precipitation

The reflective snow cover on the Prairies, with an albedo of  $\approx 0.7$ , acts as a climate switch that reduces  $T_m$  by

$10^\circ\text{C}$  (Betts et al. 2014b, 2016; Betts and Tawfik 2016). April is the month when the snowpack finally melts and the ground thaw occurs on the Prairies. For the April multiple regression analysis, we standardized all variable groups by the April SD of the mean and used the monthly SD for precipitation. The results in Table 2 below “Opaque cloud and precipitation” for the 12 stations in Alberta and Saskatchewan show the coefficients of the multiple regression of selected standardized variables on standardized anomalies of opaque cloud for April and precipitation from April back to November [A–G in Eq. (1)]. We see that the April monthly anomalies show memory of the anomalies of precipitation back 5 months through the entire cold season to November, when typically the ground begins to freeze and the first lasting snow occurs (Betts et al. 2014b).

For the first row,  $\delta\text{OPAQ}_m\text{-Apr}_{\sigma}$ , the large negative coefficients for the anomalies  $\delta\text{DTR}_{\sigma}$ ,  $\delta T_{x\sigma}$ , and  $\delta\text{P}_{\text{LCLX}\sigma}$  mean that these variables fall with increasing opaque cloud cover, while the positive sign for  $\delta\text{RH}_{n\sigma}$  and

$\delta RH_{m\sigma}$  means they increase together with opaque cloud. For  $\delta T_{x\sigma}$  and  $\delta DTR_{\sigma}$  (and  $\delta T_{m\sigma}$ , not shown), the negative coefficients  $B$ – $G$  for precipitation for the months from March back to November mean that the positive cold season precipitation anomalies are coupled to cold April temperatures. For  $\delta RH_{n\sigma}$  and  $\delta RH_{m\sigma}$  (and  $\delta RH_{x\sigma}$ , not shown), the positive coefficients  $B$ – $G$  for precipitation mean that positive cold season precipitation anomalies are coupled to higher RH in April. Most coefficients for  $\delta DTR_{\sigma}$ ,  $\delta RH_{n\sigma}$ ,  $\delta RH_{m\sigma}$ , and  $\delta P_{LCLx\sigma}$  (afternoon maximum of the pressure height of the LCL, representative of cloud base) have a 99% confidence ( $p < 0.01$ ).

There are several physical processes that are probably involved. The precipitation over the cold season is mostly stored in the snowpack until spring, when melt absorbs energy and cools the surface; the melt also provides water for evaporation, which also cools and increases RH. In addition the freeze-up of the soil in November may similarly preserve November precipitation anomalies as soil ice through the cold season until spring melt.

We assessed the role of the snowpack storage. The regression of standardized March snow-depth anomalies on precipitation anomalies from November to March is ( $R^2 = 0.38$ )

$$\delta \text{Snowdepth-Mar}_{\sigma} = (0.27 \pm 0.04)\delta \text{PR-Mar}_{\sigma} + (0.33 \pm 0.03)\delta \text{PR-Feb}_{\sigma} + (0.34 \pm 0.04)\delta \text{PR-Jan}_{\sigma} + (0.12 \pm 0.03)\delta \text{PR-Dec}_{\sigma} + (0.17 \pm 0.03)\delta \text{PR-Nov}_{\sigma}. \quad (2)$$

Not surprisingly, we see memory of precipitation anomalies, which typically fell as snow, back to

November. All coefficients in Eq. (2) have a confidence >99%.

$$\delta Y\text{-Apr}_{\sigma} = A(\delta \text{OPAQ}_m\text{-Apr}_{\sigma}) + B(\delta \text{PR-Apr}_{\sigma}) + C(\delta \text{PR-Mar}_{\sigma}) + D(\delta \text{PR-Feb}_{\sigma}) + E(\delta \text{PR-Jan}_{\sigma}) + F(\delta \text{PR-Dec}_{\sigma}) + G(\delta \text{PR-Nov}_{\sigma}) + S(\delta \text{Snowdepth-Mar}_{\sigma}). \quad (3a)$$

The second section of Table 2 below “Adding March snow-depth anomalies” shows the coefficients from Eq. (3a), which adds the standardized snow-depth anomaly for March to the April multiple regression analysis. The number of months drops from 620 to 552, because some years have no snow-depth measurements. We see the  $R^2$  values for the five variables all increase, except for  $T_x$ . The coefficients for the March snow-depth anomalies are substantial (confidence >99.9%), while the coefficients  $B$ – $G$  for the precipitation anomalies are smaller in magnitude and lower in confidence than in Table 2 below “Opaque cloud and precipitation,” understandably because the March snow depth has accumulated from the frozen winter precipitation. Our physical interpretation is that as the snowpack builds over the winter, there will be some thawing and refreezing, and the snowpack density is likely to

increase. March snow depth alone captures much, but not all of the cold season precipitation anomaly signal.

In April, however, the high albedo of the remaining snowpack plays a direct climate role, and this is a more fundamental issue. Days with no snow cover have an unstable daytime BL, while days with reflective snow cover are 10°C cooler with a stable BL and a smaller diurnal range (Betts and Tawfik 2016; Betts et al. 2016). Betts et al. (2014a) found a nearly linear relation between  $T_m$  and DRHR in March and April and the fraction of days with surface snow cover.

So we computed the standardized April snow cover frequency anomaly from the fraction of days in April with nonzero snow depth and added this to the multiple regression Eq. (1) of the April anomalies on opaque cloud and precipitation anomalies to give

$$\delta Y\text{-Apr}_{\sigma} = A(\delta \text{OPAQ}_m\text{-Apr}_{\sigma}) + B(\delta \text{PR-Apr}_{\sigma}) + C(\delta \text{PR-Mar}_{\sigma}) + D(\delta \text{PR-Feb}_{\sigma}) + E(\delta \text{PR-Jan}_{\sigma}) + F(\delta \text{PR-Dec}_{\sigma}) + G(\delta \text{PR-Nov}_{\sigma}) + T(\delta \text{Snowcover-Apr}_{\sigma}). \quad (3b)$$

Table 2 below “Adding fraction of April days with snow cover” shows the coefficients from Eq. (3b). There is an increase in  $R^2$  for all variables, and especially for  $T_x$ , where snow cover frequency anomalies have as large

an impact as opaque cloud anomalies. Note that the coefficients  $G$  for  $\delta \text{PR-Nov}_{\sigma}$  for  $\delta RH_{n\sigma}$ ,  $\delta RH_{m\sigma}$ , and  $\delta P_{LCLx\sigma}$  are not significant, but the coefficients for  $\delta DTR_{\sigma}$  and  $\delta T_{x\sigma}$  have a confidence >99% in Table 2

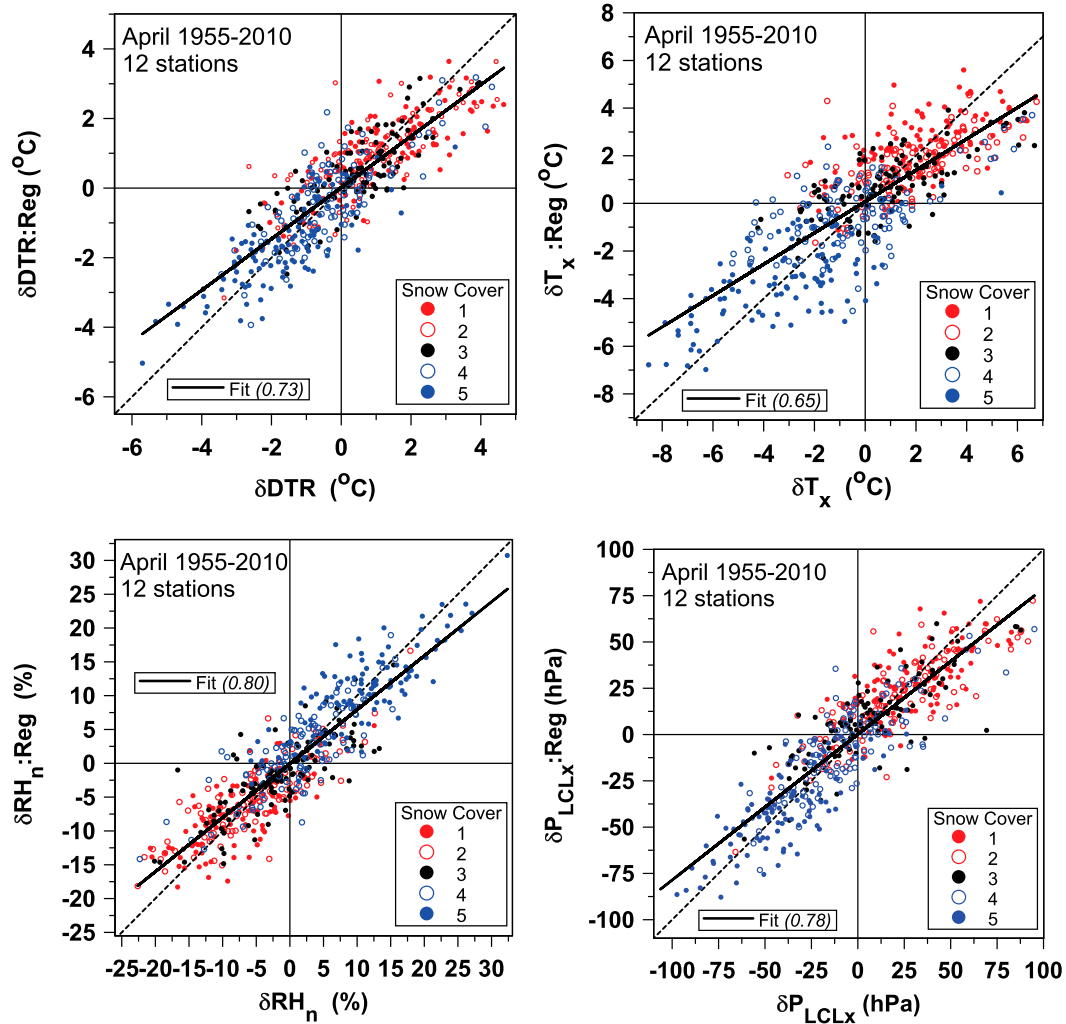


FIG. 1. Table 2 below “Adding fraction of April days with snow cover” regression fits ( $R^2$  values in parentheses) for April anomalies of (top left) DTR, (top right)  $T_x$ , (bottom left)  $\text{RH}_n$ , and (bottom right)  $P_{\text{LCLx}}$  on April opaque cloud and snow cover frequency and April–November precipitation; color sorted by quintiles of increasing standardized snow cover frequency.

when snow depth or snow cover are included. It is possible that this is the cooling impact in April coming from the melt of soil-ice frozen back in November.

Figure 1 shows the multiple regression fits from Eq. (3b) for the monthly anomalies for four variables in physical units, where we have color sorted the points by quintiles of increasing standardized snow cover frequency. The standardization has been removed by multiplying by the SD of  $\delta T_m$ ,  $\delta\text{RH}_m$ , and  $\delta P_{\text{LCLm}}$ . Figure 1 (top left) is for DTR, for which the SD of the April anomalies is 1.8°C; Fig. 1 (top right) is for  $T_x$ , for which the SD is 3.1°C; Fig. 1 (bottom left) is for  $\delta\text{RH}_n$ , for which the SD is 9.4%; and Fig. 1 (bottom right) is for  $\delta P_{\text{LCLx}}$ , for which the SD is 36.2 hPa. The multiple

regression  $R^2$  values are also the slopes of the linear fits shown. Figure 1 illustrates that large variability in the April climate is partly related to the frequency of days in April with snow cover. April mean  $T_x$ , DTR, and  $P_{\text{LCLx}}$  decrease and  $\text{RH}_n$  increases if the fraction of days with snow cover increases.

Table 2 below “Opaque cloud and precipitation” is a conventional treatment of the mean April climatology, which is itself an average of two distinct climatologies with and without snow (Betts and Tawfik 2016). So it is not surprising that mean April climate, especially  $T_x$ , has a dependence on the fraction of days in the month with snow cover, as well as cloud cover and lagged precipitation. The conventional averaging of the snow and no-snow climatologies

TABLE 3. Standardized multiple regression coefficients for the warm season monthly anomalies of  $\delta DTR_{\sigma}$ ,  $\delta RH_{ns}$ ,  $\delta P_{LCLx\sigma}$ , and  $\delta Q_{Tx\sigma}$ . For confidence notation, see Table 2.

	$\delta DTR_{\sigma}$	$\delta RH_{ns}$	$\delta P_{LCLx\sigma}$	$\delta Q_{Tx\sigma}$
<b>May</b>				
620 months $R^2$	0.74	0.72	0.72	0.23
$\delta OPAQ_m$ -May $_{\sigma}$ (A)	<b>-0.59 ± 0.02</b>	<b>0.61 ± 0.02</b>	<b>-0.78 ± 0.03</b>	(0.04 ± 0.05)
$\delta PR$ -May $_{\sigma}$ (B)	<b>-0.23 ± 0.02</b>	<b>0.33 ± 0.02</b>	<b>-0.35 ± 0.03</b>	<b>0.51 ± 0.05</b>
$\delta PR$ -Apr $_{\sigma}$ (C)	<b>-0.10 ± 0.02</b>	<b>0.13 ± 0.02</b>	<b>-0.18 ± 0.03</b>	(0.04 ± 0.04)
$\delta PR$ -Mar $_{\sigma}$ (D)	(-0.02 ± 0.02)	<b>0.07 ± 0.02</b>	<b>-0.08 ± 0.03</b>	0.07 ± 0.04
$\delta PR$ -Feb $_{\sigma}$ (E)		(0.03 ± 0.02)	(-0.03 ± 0.03)	(0.06 ± 0.04)
<b>June</b>				
617 months $R^2$	0.68	0.67	0.66	0.33
$\delta OPAQ_m$ -June $_{\sigma}$ (A)	<b>-0.53 ± 0.02</b>	<b>0.59 ± 0.03</b>	<b>-0.74 ± 0.03</b>	(0.02 ± 0.04)
$\delta PR$ -June $_{\sigma}$ (B)	<b>-0.30 ± 0.02</b>	<b>0.41 ± 0.03</b>	<b>-0.44 ± 0.03</b>	<b>0.65 ± 0.04</b>
$\delta PR$ -May $_{\sigma}$ (C)	<b>-0.17 ± 0.02</b>	<b>0.18 ± 0.02</b>	<b>-0.26 ± 0.03</b>	0.07 ± 0.04
$\delta PR$ -Apr $_{\sigma}$ (D)	(-0.03 ± 0.02)	<b>0.06 ± 0.02</b>	<b>-0.10 ± 0.03</b>	(0.02 ± 0.04)
$\delta PR$ -Mar $_{\sigma}$ (E)	-0.05 ± 0.02	0.04 ± 0.02	(-0.05 ± 0.03)	0.08 ± 0.04
<b>July</b>				
614 months $R^2$	0.68	0.61	0.62	0.26
$\delta OPAQ_m$ -July $_{\sigma}$ (A)	<b>-0.56 ± 0.03</b>	<b>0.50 ± 0.03</b>	<b>-0.63 ± 0.04</b>	(0.03 ± 0.04)
$\delta PR$ -July $_{\sigma}$ (B)	<b>-0.31 ± 0.02</b>	<b>0.37 ± 0.03</b>	<b>-0.45 ± 0.04</b>	<b>0.34 ± 0.04</b>
$\delta PR$ -June $_{\sigma}$ (C)	<b>-0.22 ± 0.02</b>	<b>0.34 ± 0.02</b>	<b>-0.44 ± 0.04</b>	<b>0.38 ± 0.04</b>
$\delta PR$ -May $_{\sigma}$ (D)	<b>-0.12 ± 0.02</b>	<b>0.11 ± 0.03</b>	<b>-0.16 ± 0.03</b>	<b>0.16 ± 0.04</b>
$\delta PR$ -Apr $_{\sigma}$ (E)	-0.04 ± 0.02	0.06 ± 0.03	-0.06 ± 0.03	<b>0.12 ± 0.04</b>
$\delta PR$ -Mar $_{\sigma}$ (F)		0.06 ± 0.03	-0.07 ± 0.03	0.10 ± 0.04
<b>August</b>				
615 months $R^2$	0.80	0.76	0.74	0.24
$\delta OPAQ_m$ -Aug $_{\sigma}$ (A)	<b>-0.68 ± 0.02</b>	<b>0.63 ± 0.03</b>	<b>-0.81 ± 0.03</b>	(-0.06 ± 0.05)
$\delta PR$ -Aug $_{\sigma}$ (B)	<b>-0.24 ± 0.02</b>	<b>0.40 ± 0.03</b>	<b>-0.45 ± 0.03</b>	<b>0.44 ± 0.05</b>
$\delta PR$ -July $_{\sigma}$ (C)	<b>-0.12 ± 0.02</b>	<b>0.22 ± 0.02</b>	<b>-0.29 ± 0.03</b>	<b>0.19 ± 0.04</b>
$\delta PR$ -June $_{\sigma}$ (D)	-0.04 ± 0.02	<b>0.12 ± 0.02</b>	<b>-0.16 ± 0.03</b>	<b>0.29 ± 0.03</b>
$\delta PR$ -May $_{\sigma}$ (E)	-0.04 ± 0.02	(0.02 ± 0.02)	-0.05 ± 0.03	-0.07 ± 0.04
$\delta PR$ -Apr $_{\sigma}$ (F)		<b>0.06 ± 0.02</b>	<b>-0.08 ± 0.03</b>	<b>0.11 ± 0.04</b>
$\delta PR$ -Mar $_{\sigma}$ (G)		<b>0.07 ± 0.02</b>	<b>-0.09 ± 0.03</b>	0.07 ± 0.04
<b>September</b>				
615 months $R^2$	0.84	0.78	0.78	0.15
$\delta OPAQ_m$ -Sep $_{\sigma}$ (A)	<b>-0.73 ± 0.02</b>	<b>0.77 ± 0.03</b>	<b>-0.99 ± 0.03</b>	<b>-0.35 ± 0.05</b>
$\delta PR$ -Sep $_{\sigma}$ (B)	<b>-0.21 ± 0.02</b>	<b>0.33 ± 0.03</b>	<b>-0.34 ± 0.03</b>	<b>0.32 ± 0.05</b>
$\delta PR$ -Aug $_{\sigma}$ (C)	<b>-0.10 ± 0.02</b>	<b>0.24 ± 0.02</b>	<b>-0.32 ± 0.03</b>	<b>0.28 ± 0.04</b>
$\delta PR$ -July $_{\sigma}$ (D)	(-0.02 ± 0.02)	0.05 ± 0.02	<b>-0.07 ± 0.03</b>	
$\delta PR$ -June $_{\sigma}$ (E)		0.04 ± 0.02	-0.06 ± 0.03	

raises fundamental issues, but we will defer these to future work.

After April the warm season memory of precipitation does not extend back through the cold season. For June–August, there is some memory of precipitation back to March (see next section).

#### 4. Warm season monthly anomaly regression fits

The warm season months May–September have no snow, and the coupling between opaque cloud cover and the diurnal ranges of  $T$ ,  $RH$ ,  $P_{LCL}$ , and  $\theta_E$  is quite uniform (Betts and Tawfik 2016). In this section, we will show the joint dependence on opaque cloud and lagged monthly precipitation.

##### a. Regression statistics by month

We derived the coefficients  $A$ – $G$  in Eq. (1) for each variable for each month, merging the six stations in Saskatchewan with the six in Alberta. Independently, the regional clusters yielded similar coefficients (not shown), and the merger reduces RMS uncertainty in the coefficients. Table 3 shows the coefficients for each month for anomalies  $\delta DTR_{\sigma}$ ,  $\delta RH_{ns}$ ,  $\delta P_{LCLx\sigma}$ , and  $\delta Q_{Tx\sigma}$ . The leading coefficients  $A$  for  $\delta DTR_{\sigma}$ ,  $\delta RH_{ns}$ , and  $\delta P_{LCLx\sigma}$  show a strong correlation to  $\delta OPAQ_m$  for the current month, with a minimum in  $A$  in June, when the solar zenith angle has a minimum. The coefficients ( $B$ – $G$ ) for precipitation show a generally decreasing dependence from the current month

TABLE 4. Standardized multiple regression coefficients for the MJJA growing season merge of 2466 months.

Variable	$A$ ( $\delta\text{OPAQ}_{m\sigma}$ )	$B$ ( $\delta\text{PR}0_{\sigma}$ )	$C$ ( $\delta\text{PR}1_{\sigma}$ )	$D$ ( $\delta\text{PR}2_{\sigma}$ )	$E$ ( $\delta\text{PR}3_{\sigma}$ )	$R^2$
$\delta T_{x\sigma}$	<b>-0.95 ± 0.02</b>	<b>-0.07 ± 0.02</b>	<b>-0.16 ± 0.02</b>	(-0.01 ± 0.02)	-0.03 ± 0.02	0.58
$\delta T_{m\sigma}$	<b>-0.67 ± 0.02</b>	<b>0.03 ± 0.02</b>	<b>-0.10 ± 0.02</b>			0.43
$\delta T_{n\sigma}$	<b>-0.34 ± 0.02</b>	<b>0.18 ± 0.02</b>	(-0.01 ± 0.02)	0.04 ± 0.02		0.13
$\delta\text{DTR}_{\sigma}$	<b>-0.61 ± 0.01</b>	<b>-0.26 ± 0.01</b>	<b>-0.15 ± 0.01</b>	<b>-0.05 ± 0.01</b>	<b>-0.03 ± 0.01</b>	0.73
$\delta\text{RH}_{n\sigma}$	<b>0.59 ± 0.01</b>	<b>0.37 ± 0.01</b>	<b>0.23 ± 0.01</b>	<b>0.09 ± 0.01</b>	<b>0.03 ± 0.01</b>	0.69
$\delta\text{RH}_{m\sigma}$	<b>0.53 ± 0.01</b>	<b>0.32 ± 0.01</b>	<b>0.24 ± 0.01</b>	<b>0.11 ± 0.01</b>	<b>0.04 ± 0.01</b>	0.61
$\delta\text{RH}_{x\sigma}$	<b>0.38 ± 0.02</b>	<b>0.20 ± 0.02</b>	<b>0.20 ± 0.01</b>	<b>0.10 ± 0.01</b>	0.04 ± 0.01	0.36
$\delta\text{DRHR}_{\sigma}$	<b>-0.22 ± 0.01</b>	<b>-0.18 ± 0.01</b>	<b>-0.03 ± 0.01</b>			0.26
$\delta Q_{T_{x\sigma}}$	(-0.01 ± 0.02)	<b>0.49 ± 0.02</b>	<b>0.22 ± 0.02</b>	<b>0.17 ± 0.02</b>		0.24
$\delta Q_{m\sigma}$	<b>-0.06 ± 0.02</b>	<b>0.41 ± 0.02</b>	<b>0.22 ± 0.02</b>	<b>0.16 ± 0.02</b>	0.03 ± 0.02	0.22
$\delta Q_{T_{n\sigma}}$	<b>-0.06 ± 0.02</b>	<b>0.33 ± 0.02</b>	<b>0.15 ± 0.02</b>	<b>0.13 ± 0.02</b>	0.03 ± 0.02	0.17
$\delta\theta_{E_{x\sigma}}$	<b>-0.55 ± 0.02</b>	<b>0.28 ± 0.02</b>	<b>0.08 ± 0.02</b>	<b>0.12 ± 0.02</b>		0.21
$\delta\theta_{E_{m\sigma}}$	<b>-0.42 ± 0.02</b>	<b>0.30 ± 0.02</b>	<b>0.09 ± 0.02</b>	<b>0.11 ± 0.02</b>		0.17
$\delta\theta_{E_{n\sigma}}$	<b>-0.22 ± 0.02</b>	<b>0.34 ± 0.02</b>	<b>0.09 ± 0.02</b>	<b>0.11 ± 0.02</b>		0.13
$\delta D\theta_E R_{\sigma}$	<b>-0.32 ± 0.01</b>	<b>-0.06 ± 0.01</b>				0.37
$\delta P_{\text{LCL}_{x\sigma}}$	<b>-0.76 ± 0.02</b>	<b>-0.42 ± 0.02</b>	<b>-0.31 ± 0.01</b>	<b>-0.13 ± 0.01</b>	<b>-0.05 ± 0.01</b>	0.68
$\delta P_{\text{LCL}_{m\sigma}}$	<b>-0.55 ± 0.01</b>	<b>-0.30 ± 0.01</b>	<b>-0.25 ± 0.01</b>	<b>-0.12 ± 0.01</b>	<b>-0.04 ± 0.01</b>	0.62
$\delta P_{\text{LCL}_{n\sigma}}$	<b>-0.30 ± 0.01</b>	<b>-0.15 ± 0.01</b>	<b>-0.16 ± 0.01</b>	<b>-0.08 ± 0.01</b>	<b>-0.03 ± 0.01</b>	0.36
$\delta\text{DP}_{\text{LCL}} R_{\sigma}$	<b>-0.46 ± 0.01</b>	<b>-0.27 ± 0.01</b>	<b>-0.15 ± 0.01</b>	<b>-0.05 ± 0.01</b>	2	0.58

to the preceding months, and memory goes back further for  $\delta\text{RH}_{n\sigma}$  and  $\delta P_{\text{LCL}_{x\sigma}}$  than for  $\delta\text{DTR}_{\sigma}$ . In contrast, afternoon mixing ratio  $\delta Q_{T_{x\sigma}}$  has very little dependence on  $\delta\text{OPAQ}_m$  until September, and a more complex dependence on precipitation. For May and June, the coefficients  $B$  for the current month are far larger than  $C$ ,  $D$ , and  $E$  for past months (where some are not significant), but for  $\delta Q_{T_{x\sigma}}$  in July, all the precipitation coefficients ( $B$ – $F$ ) have >95% confidence back to March. It is possible that precipitation memory is long in July at the peak of the growing season because rooting is deepest. Note that the variables that are strongly correlated to  $\delta\text{OPAQ}_m$  and have higher values of  $R^2$  are those that have a large diurnal cycle driven by the cloud radiative forcing. As the correlation coefficients with lagged precipitation anomalies decrease going back to earlier months, their contribution to increasing  $R^2$  values become small.

Betts et al. (2014a) showed that there is a large drawdown of total water storage on the landscape during the growing season, and Betts et al. (2013b) showed that more intensive cropping has cooled and moistened the growing season climate in the past two decades. For July and August, there is memory of precipitation anomalies back to March for  $\delta\text{RH}_{n\sigma}$ ,  $\delta P_{\text{LCL}_{x\sigma}}$ , and  $\delta Q_{T_{x\sigma}}$ , but not for  $\delta\text{DTR}_{\sigma}$ , suggesting perhaps some residual memory of snow in the water budget. This is broadly consistent with earlier modeling work that showed that spring moisture availability controls the evolution of temperature and, in some cases, precipitation during the summer months (Fennessy and Shukla 1999; Kim and

Wang 2007; Wu et al. 2007). By September, after the harvesting of annual crops (Betts et al. 2013b), this long memory shrinks back to June and July for  $\delta\text{RH}_{n\sigma}$  and  $\delta P_{\text{LCL}_{x\sigma}}$ .

#### b. Merge of May–August

Clearly there is seasonal structure in the coefficients in Table 3, and the memory of precipitation is longer in July and August. However, if we merge the growing season months MJJA for which we have 2466 months, the RMS uncertainty of the regression coefficients is reduced. This gives a unified description for the growing season coupling of the thermodynamic variables on cloud and lagged precipitation. We retain precipitation anomalies for just 4 months.

Table 4 lists our full set of standardized monthly anomalies of  $T$ ,  $\text{RH}$ ,  $Q$ ,  $\theta_E$ , and  $P_{\text{LCL}}$  and gives the standardized regression coefficients for  $A$ – $E$  in Eq. (1). The precipitation coefficients decrease going back in time, and many of them are significant at the 99% level (boldface). The coefficients for  $E$  are generally small. Note that there is a large variation in the explained variance represented by  $R^2$ .

The first groups are the regression coefficients for the temperature anomalies,  $\delta T_{x\sigma}$ ,  $\delta T_{m\sigma}$ ,  $\delta T_{n\sigma}$ , and  $\delta\text{DTR}_{\sigma}$ , which were all standardized by the SD of  $\delta T_m$ . The fit represented by  $R^2$  is largest for DTR and decreases from  $\delta T_{x\sigma}$  to  $\delta T_{n\sigma}$ . All the temperature variable anomalies show a strong inverse correlation with opaque cloud anomalies that reflect the downward SW radiation. The warm season is dominated by negative SWCF: opaque clouds reduce  $\delta T_{x\sigma}$ ,  $\delta T_{m\sigma}$ , and  $\delta\text{DTR}_{\sigma}$  (Betts et al.

2013a, 2015; Betts and Tawfik 2016). The negative values of  $A$  decrease from  $\delta T_{x\sigma}$  to  $\delta T_{n\sigma}$ . The  $\delta DTR_{\sigma}$  has a negative correlation to both cloud anomalies and to precipitation anomalies going back for 3 months. Note that because all the temperatures were standardized by the SD of  $\delta T_m$ , the coefficients for the diurnal range are the difference of the corresponding coefficients for the maximum and minimum. For example,  $A(\delta DTR_{\sigma}) = -0.61 = A(\delta T_{x\sigma}) - A(\delta T_{n\sigma})$ . Further,  $B(\delta DTR_{\sigma}) = -0.26 = B(\delta T_{x\sigma}) - B(\delta T_{n\sigma})$  (rounded to two significant figures) shows the role of the positive correlation of  $T_n$  with precipitation anomalies for the current month. We see that the coefficients  $B$  change sign in the sequence from  $\delta T_{x\sigma}$  to  $\delta T_{m\sigma}$  to  $\delta T_{n\sigma}$ . This means that although  $T_m$  falls strongly with cloud, its coupling to precipitation is weak because the coefficients  $B$  and  $C$  have opposite sign, in contrast to the RH anomalies discussed below. This regression analysis clearly shows that mean temperature anomalies  $\delta T_{m\sigma}$  are strongly coupled to cloud, and therefore solar forcing, but rather weakly to precipitation, while  $\delta DTR_{\sigma}$  (and  $\delta T_{x\sigma}$ ) decrease with both cloud and precipitation. We cannot infer causality from multiple regressions, but negative  $B$  for  $\delta T_{x\sigma}$  is consistent with evaporation from moist soils reducing  $T_x$ , and the positive  $B$  for  $\delta T_{n\sigma}$  is consistent with the fact that under wetter conditions the fall of  $T_n$  at night is limited by saturation.

The next group is the four RH anomalies,  $\delta RH_{x\sigma}$ ,  $\delta RH_{m\sigma}$ ,  $\delta RH_{n\sigma}$ , and  $\delta DRHR_{\sigma}$ . For the first three, the regression coefficients show that positive RH anomalies are correlated with positive cloud and precipitation anomalies, and the coefficients are significant for both present and three past months. The coefficients for  $\delta DRHR_{\sigma}$  are negative because  $\delta RH_{n\sigma}$  increases faster with cloud and precipitation than  $\delta RH_{x\sigma}$ , and the coefficients are significant for only one past month. The fit  $R^2$  decreases monotonically from the afternoon minimum  $\delta RH_{n\sigma}$  to  $\delta RH_{m\sigma}$  to the sunrise maximum  $\delta RH_{x\sigma}$  to  $\delta DRHR_{\sigma}$ . The diurnal cycle of  $T$  and RH have an inverse dependence on opaque cloud, reaching  $T_x$  and  $RH_n$  in the afternoon at the same time (Table 1). This is related to the fact that mixing ratio  $Q$  is tightly constrained by BL transports, which we will discuss below. But over land, near-surface RH is constrained by the availability of soil moisture for evaporation from bare soil and transpiration (which is often modeled as a stomatal resistance to evaporation; e.g., Monteith 1977; Collatz et al. 1991; Betts et al. 2004). Soil moisture anomalies are related in turn to precipitation anomalies. We see that afternoon  $RH_n$  and mean  $RH_m$  anomalies have a strong positive correlation to precipitation anomalies and a large  $R^2$ . However,  $RH_x$ , which increases with precipitation,

is limited if surface saturation is reached and dew forms before sunrise. Because the latent heat release slows the temperature fall, it is consistent that  $RH_x$  and  $T_n$  anomalies are both positively coupled to wetter precipitation anomalies for the current month (coefficient  $B$ ).

Table 4 next shows the coefficients for  $\delta Q_{Tx\sigma}$ ,  $\delta Q_{m\sigma}$ , and  $\delta Q_{Tn\sigma}$ , where  $\delta Q_{Tx}$  and  $\delta Q_{Tn}$  have been recomputed using afternoon  $T_x$ ,  $RH_n$  and sunrise  $T_n$ ,  $RH_x$  (see Table 1). The fit  $R^2$  is much smaller for all these  $Q$  variables than for RH, partly because their diurnal range is small, and their correlation to opaque cloud is very small, in fact on the order of zero for  $Q_{Tx}$ . All three  $Q$  anomalies have a positive correlation to precipitation anomalies, with a general decrease in the coefficients  $B$ ,  $C$ , and  $D$  from  $Q_{Tx}$  to  $Q_{Tn}$ . The fact that  $Q$  is correlated to precipitation anomalies, but very little to cloud, is related to the inverse diurnal dependence of  $T$  and RH on cloud. The positive coefficients  $B$ – $E$  are consistent with increased precipitation increasing evapotranspiration. The diurnal variation of mixing ratio  $Q$  has a double maxima and minima, which we will discuss in more detail in section 4d.

The next group in Table 4 shows the coefficients for  $\delta\theta_{Ex\sigma}$ ,  $\delta\theta_{Em\sigma}$ ,  $\delta\theta_{En\sigma}$ , and  $\delta D\theta_{ER\sigma}$ . The first three show the decrease with increased cloud but an increase with precipitation. The  $R^2$  values are small, even though the coefficients have 99% confidence. The diurnal range of  $\theta_E$  is dominated by the dependence of DTR on opaque cloud. The final group in Table 4 is the four  $P_{LCL}$  anomalies:  $P_{LCLx}$  is generally representative of afternoon cloud base (Betts et al. 2013a). Variable  $P_{LCL}$  is a function of  $T$  and RH, and we see that negative  $P_{LCL}$  anomalies are coupled to positive cloud and precipitation anomalies. The coefficients are largest for afternoon  $\delta P_{LCLx\sigma}$ , for which  $R^2$  is high. The coefficients for  $\delta P_{LCLx\sigma}$ ,  $\delta P_{LCLm\sigma}$ , and  $\delta P_{LCLn\sigma}$  are all 99% significant for both present and three past months, showing that cloud-base anomalies have a long memory of precipitation anomalies in the growing season. The two afternoon anomalies,  $\delta\theta_{Ex\sigma}$  and  $\delta P_{LCLx\sigma}$ , are most closely coupled to moist convective instability (not shown), which is favored by higher  $\theta_{Ex}$  and lower cloud base.

Table 4 summarizes the multiple regression correlation coefficients between warm season near-surface variables and opaque cloud and lagged precipitation and gives a quantitatively useful target for the evaluation of the coupled processes in models. Two important conceptual results emerge for this fully coupled land surface climate system on the Canadian Prairies. Monthly mean temperature anomalies are strongly correlated to opaque cloud but weakly

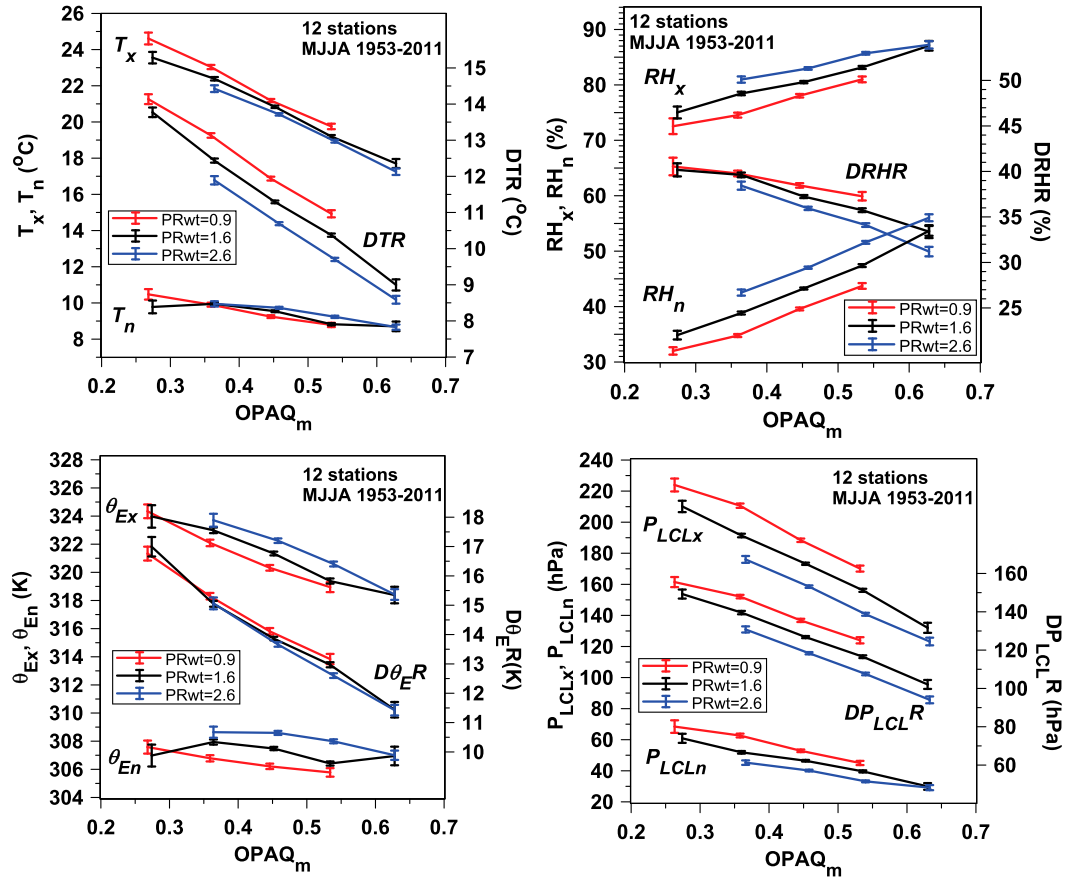


FIG. 2. Coupling between (top left) DTR,  $T_x$ , and  $T_n$ ; (top right) DRHR,  $RH_x$ , and  $RH_n$ ; (bottom left)  $D\theta_{ER}$ ,  $\theta_{Ex}$ , and  $\theta_{En}$ ; and (bottom right)  $DP_{LCLR}$ ,  $P_{LCLx}$ , and  $P_{LCLn}$  and opaque cloud fraction and weighted precipitation ( $\text{mm day}^{-1}$ ).

correlated to precipitation. Anomalies of  $Q_m$  and especially afternoon  $Q_{Tx}$  are coupled to precipitation anomalies but have little correlation to opaque cloud.

*c. Visualizing monthly climate dependence on opaque cloud and precipitation*

Betts and Tawfik (2016) showed by binning the hourly data based on daily opaque cloud cover that the warm season months (with no snow on the ground) had a very similar coupling between opaque cloud and the diurnal ranges DTR, DRHR,  $D\theta_{ER}$ , and  $DP_{LCLR}$ . Given the complexity of the land-atmosphere coupling, can we show graphically the climate dependence on precipitation as well as opaque cloud? In the previous section, we used multiple regressions to quantify the correlation of the monthly anomalies of temperature and humidity variables to anomalies of opaque cloud and precipitation. However, Table 4 shows that the coefficients for the lagged precipitation anomalies

differ considerably for different variables, so we must approximate. Following Betts et al. (2014a), we can define a simplified weighted precipitation anomaly  $\delta PR_{wt}$ , based on precipitation for just the current and the past month:

$$\delta PR_{wt} = 0.6(\delta PR_0) + 0.4(\delta PR_1). \quad (4)$$

This simplification, with this choice of coefficients in the ratio of 1.5, captures much of the precipitation dependence for the variables that have the highest  $R^2$ , such as DTR,  $RH_n$ , and  $P_{LCLx}$ , because these have the ratio of the coefficients  $B/C \approx 1.5$  in Table 4.

The  $x$  axis of Fig. 2 is 0.1 bins of  $OPAQM = \delta OPAQM + 0.46$ , where 0.46 is the mean opaque cloud over all the months. For each MJJA month (total 2466 months) we computed  $\delta PR_{wt}$  from Eq. (4) and added the MJJA mean precipitation rate of  $1.8 \text{ mm day}^{-1}$  to give  $PR_{wt} = \delta PR_{wt} + 1.8$ . We then stratified the data into three ranges of  $PR_{wt}$  of  $<1.2$ ,  $1.2\text{--}2$ , and  $>2 \text{ mm day}^{-1}$ , which have mean values of 0.9, 1.6, and  $2.6 \text{ mm day}^{-1}$ . There are (531, 1103, and

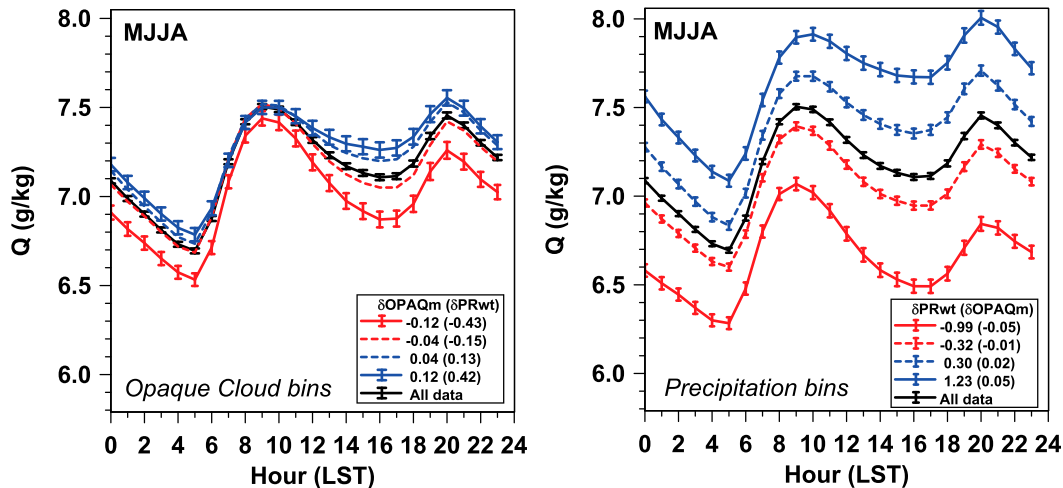


FIG. 3. Dependence of diurnal cycle of  $Q$  on (left) opaque cloud bins and (right) weighted precipitation bins.

832) months in these three  $PR_{wt}$  bins. To generate Fig. 2, we compute for each variable bin the mean and standard error (SE) of the anomalies and add back the MJJA variable means.

Figure 2 (top left) shows DTR and its components  $T_x$  and  $T_n$ ; Fig. 2 (top right) shows DRHR,  $RH_x$ , and  $RH_n$ ; Fig. 2 (bottom left) shows  $D\theta_E R$ ,  $\theta_{Ex}$ , and  $\theta_{En}$ ; and Fig. 2 (bottom right) shows  $DP_{LCL}R$ ,  $P_{LCLx}$ , and  $P_{LCLn}$ . The strong dependence on opaque cloud (Betts and Tawfik 2016) clearly dominates most of these climate variables, since  $T$  falls and  $RH$  increases with increasing cloud. This in turn is connected to the weak dependence of  $Q$  on cloud (Table 4 and section 4d). The color scheme is red and blue, respectively, for the dry and wet weighted precipitation bins. As  $PR_{wt}$  falls, DTR increases faster than  $T_x$ .

Figure 2 (top right) shows that  $RH_x$  and  $RH_n$  (and  $RH_m$ , not shown) increase with both cloud and  $PR_{wt}$ , but because afternoon  $RH_n$  increases faster than  $RH_x$ , DRHR decreases with increasing  $PR_{wt}$ . Note the rise of  $RH_x$  with  $PR_{wt}$  toward saturation. If  $RH_x$  reaches saturation at the surface on individual days, condensation of dew and the release of latent heat limit the fall of  $T_n$ .

Figure 2 (bottom) shows the variables that determine the BL coupling to clouds and precipitation. Afternoon  $P_{LCLx}$  and  $\theta_{Ex}$  determine the cloud-base height and moist adiabat. Both  $\theta_{Ex}$  and  $\theta_{En}$  increase with  $PR_{wt}$ , but the diurnal range  $D\theta_E R$  depends primarily on cloud. All the  $P_{LCL}$  variables decrease with increasing  $PR_{wt}$ . The sunrise minimum of  $P_{LCLn}$  falls with  $PR_{wt}$ , as the surface moves toward saturation. So higher precipitation, which we can loosely associate with increased daytime evaporation, corresponds

with a lower monthly mean cloud base and higher  $\theta_E$  in the afternoon, which would both favor increased convective instability.

#### d. The dependence of the diurnal cycle of $Q$ on opaque cloud and precipitation

In the warm season, the diurnal cycle of mixing ratio  $Q$  has two maxima and minima, except under cloudy conditions (Betts et al. 2013a; Betts and Tawfik 2016). There is a sunrise minimum, a rise to a midmorning maximum while evaporation is trapped beneath the nocturnal inversion, then a fall to an afternoon minimum, as water vapor is rapidly transported upward into a deep daytime BL and into clouds, and a rise again to an evening maximum as the surface layer cools and uncouples from the deep BL. We have seen in section 4b that  $Q_{Tx}$ ,  $Q_m$ , and  $Q_{Tn}$  depend on precipitation anomalies (although regression  $R^2$  are small), but have only weak dependence on opaque cloud (Table 4). The diurnal range of  $Q$  is relatively small, but we can graph its dependence on anomalies of opaque cloud cover (i.e.,  $\delta OPAQ_m$ ) and weighted precipitation anomalies (i.e.,  $\delta PR_{wt}$ ;  $\text{mm day}^{-1}$ ), derived from Eq. (4).

Figure 3 (left), derived from the MJJA growing season merge, shows the stratification by  $\delta OPAQ_m$  into four ranges:  $\delta OPAQ_m$  less than  $-0.08$ , from  $-0.08$  to  $0$ , from  $0$  to  $0.08$ , and greater than  $0.08$ , based on the SD of  $\delta OPAQ_m \approx 0.08$ . There are (371, 839, 909, and 347) months in these respective bins. We averaged in bins the diurnal cycle of the anomalies from the station monthly means, calculate the SE, and add back the 12-station MJJA mean of  $Q$ . The legend shows the mean value for each  $\delta OPAQ_m$  bin, and in parentheses the corresponding mean of  $\delta PR_{wt}$ . As mean  $\delta OPAQ_m$  increases from  $-0.12$

to  $+0.12$ , mean  $\delta PR_{wt}$  increases from  $-0.43$  to  $+0.42 \text{ mm day}^{-1}$ , and there is a small increase in  $Q_m$ .

The sunrise minimum of  $Q$  occurs at the minimum temperature, when the nighttime BL is shallow with a strong temperature inversion (Table 1). As the surface net radiation turns positive after sunrise, it drives increasing surface sensible and latent heat fluxes. This warms and moistens a shallow ML under the stable inversion, and there is a steep rise of  $Q$ . When the surface potential temperature reaches that of the top of the capping inversion in midmorning, the ML deepens more quickly, usually into a residual deep ML from the previous day, mixing with drier air from above, and so  $Q$  falls to the afternoon minimum. With less cloud and more solar forcing, the ML can grow deeper, and mix with more dry air from above, so the fall of  $Q$  is a little larger (Fig. 3).

Figure 3 (right) is the corresponding partition into four ranges of weighted precipitation anomalies:  $\delta PR_{wt}$  less than  $-0.7$ , from  $-0.7$  to  $0$ , from  $0$  to  $0.7$ , and greater than  $0.7 \text{ mm day}^{-1}$ , based on the SD of  $\delta PR_{wt} \approx 0.7 \text{ mm day}^{-1}$ . There are (387, 961, 745, and 373) months in these respective bins. The legend shows the mean value for each  $\delta PR_{wt}$  bin, and in parentheses the corresponding mean of  $\delta OPAQ_m$ . With increasing  $\delta PR_{wt}$ , there is a large upward shift of the mean diurnal cycle of  $Q$ , as  $Q_m$  increases with precipitation anomalies, which we can associate with increased soil moisture and evaporation. As mean  $\delta PR_{wt}$  increases from  $-0.99$  to  $+1.23 \text{ mm day}^{-1}$ , mean  $\delta OPAQ_m$  increases from  $-0.05$  to  $+0.05$ , and the fall of  $Q$  from midmorning maximum to afternoon minimum is reduced as in Fig. 3 (left). Clearly we are dealing with a fully coupled system, but Fig. 3 shows that climatologically the amplitude of the diurnal cycle of  $Q$  increases a little with reduced cloud cover (increased solar forcing and vertical mixing), and there is a large upward shift in the diurnal cycle with increased weighted precipitation, presumably from increased evaporation.

Figure 4 shows the separate months with the same  $PR_{wt}$  partition as Fig. 3 (right). There is a significant seasonal cycle, and the range of  $Q$  has peak amplitude in July in the middle of the growing season.

#### e. Nonlinear change of regression coefficients from wet to dry conditions

Betts et al. (2014a) showed that in the growing season on the Prairies the impact of precipitation anomalies is damped by  $56\% \pm 9\%$  by the uptake of total water storage, as measured by the Gravity Recovery and Climate Experiment (GRACE): that is, the water uptake increases when precipitation anomalies are negative and vice versa. Stratifying the regression analysis by precipitation anomalies supports this conclusion.

There are 2466 station months in the MMJA merge of the Prairie data, sufficient to further split the multiple regression analysis into ranges based on precipitation anomalies for the current month ( $\delta PR_0$ ). For the MJJA  $\delta PR_0$  precipitation anomalies, the SD (indicated by  $\sigma$ ) is  $1.1 \text{ mm day}^{-1}$ , so we split the data into four dry to wet ranges: (less than  $-1\sigma$ , from  $-1\sigma$  to  $0$ , from  $0$  to  $1\sigma$ , and greater than  $1\sigma$ ), which contain (331, 1069, 724, and 342) months, respectively.

Figure 5 shows the multiple regression coefficients  $A$ – $C$  for  $RH_n$  and DTR as a function of precipitation anomaly. All coefficients have a 99.9% confidence. The values just above the  $x$  axis are the mean monthly precipitation in millimeters per month for each range. The coefficients  $A$  for the dependence on opaque cloud show an upward change with increasing precipitation in the wettest part of the range. However, the precipitation coefficients  $B$  ( $\delta PR_0$ ) for the current month show a strong asymmetric response, increasing as monthly precipitation decreases in magnitude from 3.8 (very wet conditions) to  $1.3 \text{ mm day}^{-1}$  (slightly dry conditions, as the mean of all months is  $1.8 \text{ mm day}^{-1}$ ). This change in  $B$  implies an increased sensitivity of DTR,  $RH_n$  (and by inference evapotranspiration) to precipitation anomalies from very wet to slightly dry conditions. This is consistent with the increase in total surface water extraction from wet to dry conditions shown by the GRACE data (Betts et al. 2014a). However, under very dry conditions ( $PR_0 = 0.4 \text{ mm day}^{-1}$ ), the  $B$  coefficients decrease slightly and the standard deviation is larger. This suggests that with a month-long drought, soil moisture extraction by roots is less able to maintain evaporation, with a measurable climate impact on DTR and  $RH_n$ .

The solid squares in Fig. 5 are the mean coefficients for  $A$ – $C$  from Table 4 for MJJA. The solid red and blue squares show that the multiple linear regression does a relatively good job approximating mean values for  $A$  and  $C$ , which show the least variation with precipitation anomaly. However the solid black squares  $B$  for both DTR and  $RH_n$ , corresponding with  $PR_0$  are a poor fit to the nonlinear coupling. We conclude that the linear analysis of the full dataset is only an approximation for many complex nonlinear processes, involving the growing season phenology of crop and root growth, as well as the stomatal response to light, atmospheric conditions, and soil moisture.

## 5. Correlation between cloud and climate variables

The previous sections are framed in terms of the dependence of climate variables on opaque cloud and lagged precipitation. But since the ability of models to predict cloud may be a limiting factor in seasonal forecasting and climate change projections, the inverse

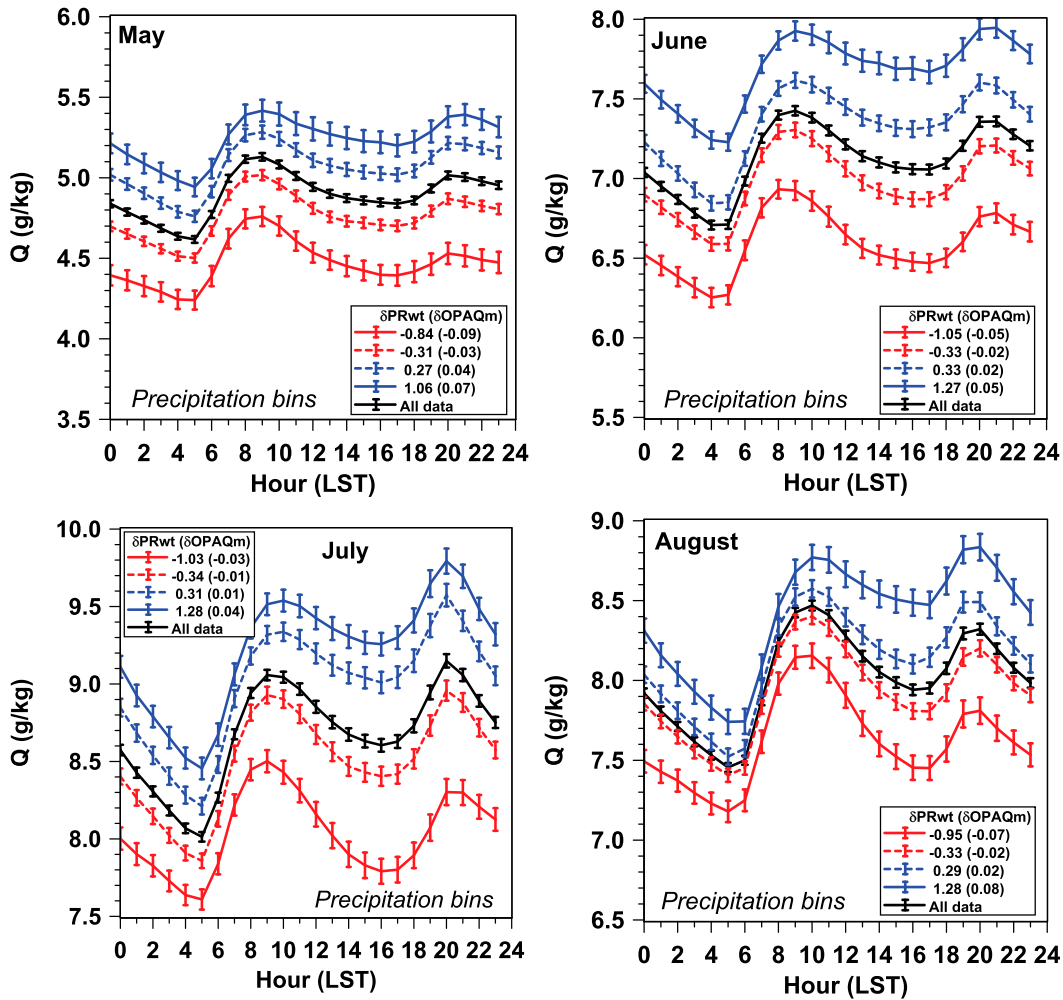


FIG. 4. Seasonal cycle of diurnal cycle of  $Q$ , stratified by weighted precipitation.

problem is also of interest. How tightly is opaque cloud cover coupled to precipitation and other climate variables?

The regression of standardized opaque cloud anomalies on the standardized monthly precipitation anomalies for the MJJAS set of 12 stations (3081 months) is

$$\delta OPAQ_{m\sigma} = 0.48(\pm 0.02)\delta PR_{0\sigma} \quad (R^2 = 0.23). \quad (5)$$

The regression of standardized opaque cloud anomalies on the standardized monthly climate anomalies  $\delta DTR_{\sigma}$ ,  $\delta T_{m\sigma}$ , and  $\delta RH_{m\sigma}$  is

$$\delta OPAQ_{m\sigma} = -0.64(\pm 0.02)\delta DTR_{\sigma} - 0.23(\pm 0.01)\delta T_{m\sigma} + 0.11(\pm 0.01)\delta RH_{m\sigma}, \quad (6)$$

with  $R^2 = 0.72$ , much higher than Eq. (5). All the coefficients in both Eqs. (5) and (6) are significant above the 99.9% level. If  $\delta PR_{0\sigma}$  is added to the regression

Eq. (6), its coefficient is on the order of zero and  $R^2$  is unchanged, meaning that the precipitation information is already contained in the three climate variables. Figure 6 shows the opaque cloud regression Eq. (5) on precipitation (Fig. 6, left) and regression Eq. (6) (Fig. 6, right) on the climate variables. The unstandardized cloud cover anomalies have been retrieved by multiplying by the SD of  $OPAQ_m = 0.084$ . For both, the linear regression fit has the same slope as the  $R^2$ . Although Fig. 6 contains no more information than Eqs. (5) and (6), we show it for its conceptual importance. Figure 6 (left) shows that cloud cover is weakly coupled to precipitation data on monthly time scales, while Fig. 6 (right) in contrast shows that opaque cloud cover is tightly coupled to three other climate variables that are routinely observed.

We cannot separate cause and effect in this fully coupled system. However, Eq. (6) flags three important issues. First is the strong inverse correlation of mean

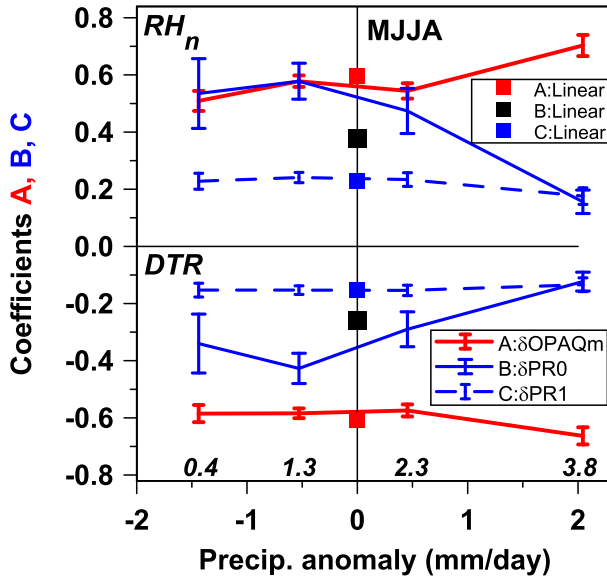


FIG. 5. Dependence of MJJA regression coefficients on precipitation anomaly  $\delta PR_0$  for the current month. The values just above the x axis are the mean monthly precipitation ( $\text{mm month}^{-1}$ ) for each group. The solid squares are the A–C linear regression coefficients from Table 4.

opaque cloud cover and DTR, which we have seen earlier in Table 4. This has long been known (e.g., Dai et al. 1999). The second is the small climate correlation between increases of  $OPAQ_m$  with  $RH_m$ , which from a physical perspective is not surprising. The third is the inverse correlation between  $OPAQ_m$  and  $T_m$ . This is of potential importance, since if there is a decrease in cloud cover over land with increasing temperature, this is a potential positive climate feedback. This has been seen in the idealized coupled equilibrium model of Betts and

Chiu (2010), so it deserves further analysis with fully coupled models. However, we cannot draw conclusions here because these data contain seasonal variability and decadal changes that have been impacted by intensification of land use (Betts et al. 2013b).

**6. Discussion and conclusions**

The Canadian Prairie dataset with hourly opaque cloud observations as well as standard meteorological observations has transformed our understanding of hydrometeorology, because the cloud observations are good enough to represent the daily LW and SW cloud forcing of the diurnal cycle over land (Betts and Tawfik 2016). This analysis uses multiple linear regression of standardized monthly anomalies, computed from 620 station years of hourly Prairie climate data to calculate the correlation coefficients between monthly climate anomalies and opaque cloud, a surrogate for radiation, and lagged precipitation anomalies, a much weaker surrogate for soil moisture. We find that while monthly climate is strongly influenced by cloud cover for the current month, it also has memory of precipitation anomalies going back for many months.

Starting with April at the end of snowmelt, we find that April climate anomalies of  $T$ ,  $RH$ ,  $Q$ , and  $P_{LCL}$  have memory of precipitation anomalies back 5 months to freeze-up in November. Increased opaque cloud cover for April is coupled to cooler temperatures and higher  $RH$ , which is consistent with the SWCF. Increased cold season precipitation from November to March is coupled to a cooler and moister April climate with a lower afternoon LCL. Here several physical processes are probably involved. The memory of

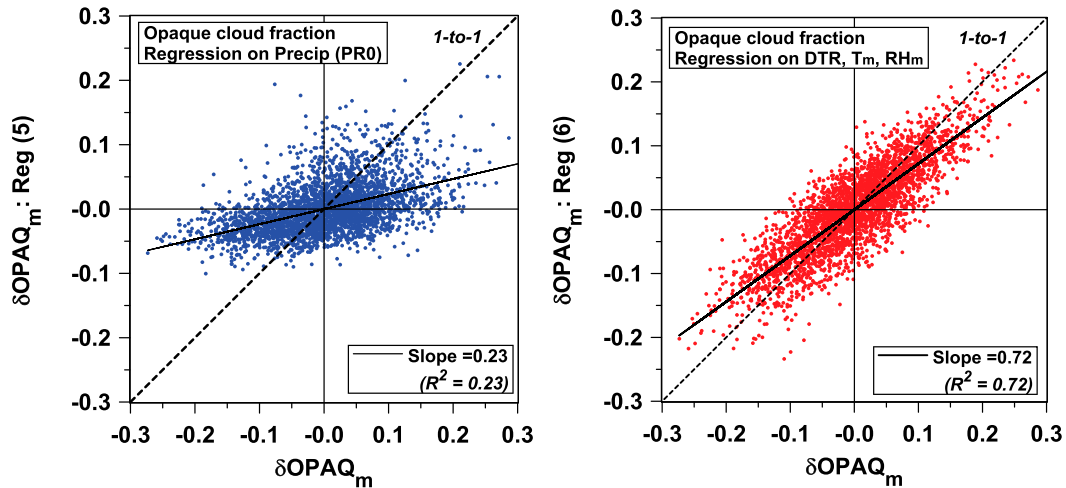


FIG. 6. Regression of  $\delta OPAQ_m$  on (left) precipitation from Eq. (5) and (right) climate variables from Eq. (6) with linear fits.

precipitation anomalies over the cold season is mostly stored in the snowpack till spring, when melt absorbs energy and cools the surface, and the melt also provides water for evaporation, which also cools temperature and increases RH. In addition the freeze-up of the soil in November may similarly preserve November precipitation anomalies as soil ice through the cold season till spring melt.

However, reflection by the high albedo of the remaining snowpack also plays a role. We found that including the fraction of days in April with snow cover, along with cloud cover and lagged precipitation in these multiple regressions for the mean April climate anomalies, increases  $R^2$  values, especially for maximum temperature. This is not surprising, given the role of reflective snow cover as a fast climate switch between different climatologies (Betts et al. 2014b; Betts and Tawfik 2016), but this raises fundamental issues about the conventional monthly averaging of these snow and no-snow climatologies, which we will defer to future work.

For all the warm season months, increased opaque cloud cover is again coupled to cooler temperatures and higher RH, but the memory of lagged precipitation anomalies is longest in July and August, probably because crop rooting is deepest. The climates in MJJA have memory of precipitation anomalies back to the beginning of snowmelt in March. In September, after the harvest of crops, precipitation memory goes back weakly only to June.

We merged the months MJJA in order to calculate a single set of coefficients that couple all the growing season climate anomalies to opaque cloud and precipitation for the current month and precipitation for three preceding months. In the warm season,  $T_m$  is strongly correlated to opaque cloud anomalies, but only weakly to precipitation anomalies. Mixing ratio anomalies are correlated to precipitation, but only weakly to cloud. The full sets of coefficients given in Table 4 provide a useful measure of the behavior of the fully coupled system.

To show graphically the coupled dependence of the diurnal ranges of  $T$ , RH,  $\theta_E$ , and  $P_{LCL}$ , we stratify by opaque cloud and a simplified weighted precipitation, calculated from only the precipitation for the current and preceding month. The monthly climate dependence on opaque cloud dominates (Betts and Tawfik 2016), and  $T$  falls and RH increases with increasing cloud. This in turn is connected to the very weak dependence of  $Q$  on cloud. As weighted precipitation falls, DTR increases faster than  $T_x$ , while afternoon  $RH_n$  falls faster than  $RH_x$ . Higher precipitation anomalies are coupled to a lower afternoon LCL, a surrogate for cloud base, and a higher afternoon equivalent potential temperature, which both favor increased convection and precipitation. The

diurnal cycle of  $Q$  shifts strongly upward with increasing precipitation anomalies, and the fall of  $Q$  from morning maximum to afternoon minimum decreases with increasing opaque cloud.

When the growing season is stratified by precipitation anomaly for the current month, we find that the coupling varies with precipitation. Regression coefficients on the current month precipitation anomalies increase from wet to slightly dry conditions, until drought conditions are reached. This is consistent with increased uptake of soil water when monthly precipitation is low, in agreement with satellite observations from GRACE (Betts et al. 2014b). This nonlinear system behavior shows the limits of multiple linear regression. The linear analysis of the full dataset is only an approximation for many complex nonlinear processes, involving the growing season phenology of crop growth, the stomatal response to light, atmospheric conditions and soil moisture, and extremes of precipitation.

To explore the inverse problem, which is the correlation of cloud anomalies to climate anomalies, we performed a multiple regression analysis of monthly opaque cloud cover on monthly climate variables DTR,  $T_m$ , and  $RH_m$ . The resulting  $R^2 = 0.72$  confirms the tight relationship in the fully coupled land–BL system. Adding monthly precipitation provides no more skill, suggesting that all the available information is already embedded within DTR,  $T_m$ , and  $RH_m$ .

The work presented here is important because it confirms observationally that the coupled land–atmosphere–cloud system remembers precipitation anomalies for as long as 5 months. This means that increases in seasonal forecasting skill may be possible with improved representation of cloud and precipitation coupling in models. Similar regression analyses to those presented in this paper using cloud and climate observations may be applied to model outputs, as a strategy to evaluate the model realism in order to improve the representation of the land–BL–cloud–atmosphere system in both forecast and climate models.

*Acknowledgments.* This research was supported by Agriculture and Agri-Food Canada, and by NSF OIA 1556770 to the University of Vermont. A portion of this work was supported by the Earth System Modeling National Science Foundation Award 1419445 and the U.S. Department of Agriculture Collaborative Research Award 108923. We thank the civilian and military technicians of the Meteorological Service of Canada and the Canadian Forces Weather Service, who have made reliable cloud observations hourly for 60 years. We thank Donna Rizzo and three reviewers for helpful suggestions.

## REFERENCES

- Baldocchi, D. D., 2003: Assessing the eddy covariance technique for evaluating carbon dioxide exchange rates of ecosystems: Past, present and future. *Global Change Biol.*, **9**, 479–492, doi:10.1046/j.1365-2486.2003.00629.x.
- Betts, A. K., 2004: Understanding hydrometeorology using global models. *Bull. Amer. Meteor. Soc.*, **85**, 1673–1688, doi:10.1175/BAMS-85-11-1673.
- , and J. C. Chiu, 2010: Idealized model for changes in equilibrium temperature, mixed layer depth, and boundary layer cloud over land in a doubled CO<sub>2</sub> climate. *J. Geophys. Res.*, **115**, D19108, doi:10.1029/2009JD012888.
- , and A. B. Tawfik, 2016: Annual climatology of the diurnal cycle on the Canadian Prairies. *Front. Earth Sci.*, **4**, doi:10.3389/feart.2016.00001.
- , J. H. Ball, A. C. M. Beljaars, M. J. Miller, and P. Viterbo, 1996: The land surface-atmosphere interaction: A review based on observational and global modeling perspectives. *J. Geophys. Res.*, **101**, 7209–7225, doi:10.1029/95JD02135.
- , B. Helliker, and J. Berry, 2004: Coupling between CO<sub>2</sub>, water vapor, temperature and radon and their fluxes in an idealized equilibrium boundary layer over land. *J. Geophys. Res.*, **109**, D18103, doi:10.1029/2003JD004420.
- , R. Desjardins, and D. Worth, 2013a: Cloud radiative forcing of the diurnal cycle climate of the Canadian Prairies. *J. Geophys. Res. Atmos.*, **118**, 8935–8953, doi:10.1002/jgrd.50593.
- , —, —, and D. Cerkowniak, 2013b: Impact of land use change on the diurnal cycle climate of the Canadian Prairies. *J. Geophys. Res. Atmos.*, **118**, 11 996–12 011, doi:10.1002/2013JD020717.
- , —, —, and B. Beckage, 2014a: Climate coupling between temperature, humidity, precipitation and cloud cover over the Canadian Prairies. *J. Geophys. Res. Atmos.*, **119**, 13 305–13 326, doi:10.1002/2014JD022511.
- , —, —, S. Wang, and J. Li, 2014b: Coupling of winter climate transitions to snow and clouds over the Prairies. *J. Geophys. Res. Atmos.*, **119**, 1118–1139, doi:10.1002/2013JD021168.
- , —, A. C. M. Beljaars, and A. Tawfik, 2015: Observational study of land-surface-cloud-atmosphere coupling on daily timescales. *Front. Earth Sci.*, **3**, doi:10.3389/feart.2015.00013.
- , —, and D. Worth, 2016: The impact of clouds, land use and snow cover on climate in the Canadian Prairies. *Adv. Sci. Res.*, **13**, 37–42, doi:10.5194/asr-13-37-2016.
- BSRN, 2016: World Radiation Monitoring Center. Baseline Surface Radiation Network, Accessed 24 August 2016. [Available online at <http://bsrn.awi.de/>.]
- Collatz, G. J., J. T. Ball, C. Griivet, and J. A. Berry, 1991: Physiological and environmental regulation of stomatal conductance, photosynthesis, and transpiration: A model that includes a laminar boundary layer. *Agric. For. Meteorol.*, **54**, 107–136, doi:10.1016/0168-1923(91)90002-8.
- Dai, A., K. E. Trenberth, and T. R. Karl, 1999: Effects of clouds, soil moisture, precipitation, and water vapor on diurnal temperature range. *J. Climate*, **12**, 2451–2473, doi:10.1175/1520-0442(1999)012<2451:ECSMP>2.0.CO;2.
- Ek, M. B., and A. A. M. Holtslag, 2004: Influence of soil moisture on boundary layer cloud development. *J. Hydrometeorol.*, **5**, 86–99, doi:10.1175/1525-7541(2004)005<0086:IOSMOB>2.0.CO;2.
- Fennessy, M. J., and J. Shukla, 1999: Impact of initial soil wetness on seasonal atmospheric prediction. *J. Climate*, **12**, 3167–3180, doi:10.1175/1520-0442(1999)012<3167:IOISWO>2.0.CO;2.
- Ferguson, C. R., E. F. Wood, and R. K. Vinukollu, 2012: A global intercomparison of modeled and observed land-atmosphere coupling. *J. Hydrometeorol.*, **13**, 749–784, doi:10.1175/JHM-D-11-0119.1.
- Kim, Y., and G. Wang, 2007: Impact of initial soil moisture anomalies on subsequent precipitation over North America in the coupled land-atmosphere model CAM3-CLM3. *J. Hydrometeorol.*, **8**, 513–533, doi:10.1175/JHM611.1.
- Koster, R. D., and M. J. Suarez, 2001: Soil moisture memory in climate models. *J. Hydrometeorol.*, **2**, 558–570, doi:10.1175/1525-7541(2001)002<0558:SMMICM>2.0.CO;2.
- , and S. P. P. Manahama, 2012: Land surface controls on hydroclimatic means and variability. *J. Hydrometeorol.*, **13**, 1604–1619, doi:10.1175/JHM-D-12-050.1.
- , and Coauthors, 2010: Contribution of land surface initialization to subseasonal forecast skill: First results from a multi-model experiment. *Geophys. Res. Lett.*, **37**, L02402, doi:10.1029/2009GL041677.
- , and Coauthors, 2011: The Second Phase of the Global Land-Atmosphere Coupling Experiment: Soil moisture contributions to subseasonal forecast skill. *J. Hydrometeorol.*, **12**, 805–822, doi:10.1175/2011JHM1365.1.
- Monteith, J. L., 1977: Climate and the efficiency of crop production in Britain. *Philos. Trans. Roy. Soc. London*, **281B**, 277–294, doi:10.1098/rstb.1977.0140.
- Pal, J. S., and E. A. B. Eltahir, 2001: Pathways relating soil moisture conditions to future summer rainfall within a model of the land-atmosphere system. *J. Climate*, **14**, 1227–1241, doi:10.1175/1520-0442(2001)014<1227:PRSMCT>2.0.CO;2.
- Tuttle, S., and G. Salvucci, 2016: Empirical evidence of contrasting soil moisture-precipitation feedbacks across the United States. *Science*, **352**, 825–828, doi:10.1126/science.aaa7185.
- Van den Hurk, B., F. Doblas-Reyes, G. Balsamo, R. D. Koster, S. I. Seneviratne, and H. Camargo Jr., 2012: Soil moisture effects on seasonal temperature and precipitation forecast scores in Europe. *Climate Dyn.*, **38**, 349–362, doi:10.1007/s00382-010-0956-2.
- Webb, M. J., and Coauthors, 2006: On the contribution of local feedback mechanisms to the range of climate sensitivity in two GCM ensembles. *Climate Dyn.*, **27**, 17–38, doi:10.1007/s00382-006-0111-2.
- , F. H. Lambert, and J. M. Gregory, 2013: Origins of differences in climate sensitivity, forcing and feedback in climate models. *Climate Dyn.*, **40**, 677–707, doi:10.1007/s00382-012-1336-x.
- Wu, W., R. E. Dickinson, H. Wang, Y. Liu, and M. Shaikha, 2007: Covariabilities of spring soil moisture and summertime United States precipitation in a climate simulation. *Int. J. Climatol.*, **27**, 429–438, doi:10.1002/joc.1419.
- Xie, S., and Coauthors, 2010: ARM climate modeling best estimate data: A new data product for climate studies. *Bull. Amer. Meteor. Soc.*, **91**, 13–20, doi:10.1175/2009BAMS2891.1.